



# Environmental remediation of Direct Blue dye solutions by photocatalytic oxidation with cuprous oxide



E.S. Aazam<sup>a</sup>, R.M. Mohamed<sup>a,b,\*</sup>

<sup>a</sup>Chemistry Department, Faculty of Science, King Abdulaziz University, Jeddah, Saudi Arabia

<sup>b</sup>Advanced Materials Department, Central Metallurgical R&D Institute, CMRDI, P.O. Box 87, Helwan, Cairo, Egypt

## ARTICLE INFO

### Article history:

Received 16 April 2013

Received in revised form 8 June 2013

Accepted 27 June 2013

Available online 5 July 2013

### Keywords:

Cuprous oxide

Visible photocatalyst

Removal of Direct Blue dye

## ABSTRACT

A simple hydrothermal route has been developed to synthesize shape-controllable Cu<sub>2</sub>O from starting materials of CuCl<sub>2</sub>·2H<sub>2</sub>O and NaOH by changing the hydrothermal temperature from 80 to 140 °C. Cu<sub>2</sub>O nanorods, a mixture of nanorods and nanocubes or nanocubes have been synthesized by controlling the hydrothermal temperature. The experiments demonstrate that the hydrothermal temperature is an important parameter that may determine whether the Cu<sub>2</sub>O is shaped as nanorods, a mixture of nanorods and nanocubes or nanocubes. The products were characterized with X-ray diffraction (XRD), ultraviolet and visible spectroscopy (UV–vis), transmission electron microscopy (TEM) and surface area measurements. Furthermore, the photocatalytic performance of Cu<sub>2</sub>O was measured in the degradation of Direct Blue dye with visible light.

© 2013 Elsevier B.V. All rights reserved.

## 1. Introduction

Advanced oxidation processes (AOPs), such as heterogeneous photocatalysis, have gained a great deal of attention. TiO<sub>2</sub> is the most popular material for these processes because of its high photocatalytic activity, good photostability, lack of toxicity, and low price. However, the large band gap of TiO<sub>2</sub>, which is 3.2 eV, has proven to be a major drawback; wavelengths below 400 nm are necessary for excitation, and this requirement limits the efficiency of TiO<sub>2</sub> with solar light sources. Therefore, modifying the band gap of TiO<sub>2</sub> would help improve the optical properties of this material. In recent decades, doping with both metals and nonmetals has been successfully utilized to shift the optical response of catalytically active TiO<sub>2</sub> from the UV to the visible light region. Zeolite [1,2], graphene [3], F [4], Sm [5], Ni [6], Pt [7–9], Au [10], Ag [11,12], rare earth dopants [13,14], and Co, Cr and Ag [13,15] have been used to extend the photoresponsive range of the TiO<sub>2</sub> matrix. Cu<sub>2</sub>O has been widely exploited for use in photocatalysis and as a photoelectrode in electrochemical cells [16]. Especially under irradiation by visible light, the water-splitting activity of Cu<sub>2</sub>O to produce hydrogen fuel has been the focus of many debates [17–20]. Cu<sub>2</sub>O has also been widely exploited for use in antifouling, gas sensors, magnetic storage devices and micro–nano electronics [21,22], biosensing, and catalysis. Cu<sub>2</sub>O nanoparticles have also been used

as photocatalysts for the photocatalytic degradation of methyl orange [23,24].

Over the past decade, one-dimensional (1D) nanostructures, such as nanotubes [25], inorganic nanorods and nanowires [26–28] have attracted considerable attention. Much effort has been directed toward understanding the electronic, magnetic and optical properties of these nanostructures because they exhibit physical and chemical properties different from those of their bulk counterparts. It has been found that the properties of these nanostructures mainly depend on the sizes and shapes of the structures. Thus, one of the challenges in the synthesis of nanocrystals is to control not only the sizes but also the shapes and morphologies of the crystals [29].

Cu<sub>2</sub>O is a nonstoichiometric p-type semiconductor and is inexpensive and abundantly available. It has a direct band gap of 2.2 eV [30] and a high optical absorption coefficient, and its theoretical solar cell conversion efficiency is more than 13% [31]. Cu<sub>2</sub>O has been used in hydrogen production [32] under visible light, in solar cells [33], and in negative electrode materials for lithium ion batteries [34]. It also has a great potential in the photocatalytic degradation of organic pollutants under visible light [35]. Over the past several years, 1D nanoscale Cu<sub>2</sub>O has been synthesized by chemical deposition [36], electrodeposition [37,38] and template methods [39]. CTAB has also been used as a template to synthesize Cu<sub>2</sub>O nanotubes and nanorods [40].

The purpose of this paper was twofold: to synthesize shape-controllable Cu<sub>2</sub>O under alkaline conditions with hydrothermal methodology and to measure and evaluate the application of Cu<sub>2</sub>O to the photocatalytic degradation of the dye Direct Blue 53.

\* Corresponding author at: Chemistry Department, Faculty of Science, King Abdulaziz University, Jeddah, Saudi Arabia. Tel.: +966 540715648; fax: +966 2 6952292.

E-mail address: [redama123@yahoo.com](mailto:redama123@yahoo.com) (R.M. Mohamed).

## 2. Experiments

### 2.1. Catalyst preparation

All of the chemical reagents used in this experiment were analytical grade.  $\text{Cu}_2\text{O}$  was synthesized as follows: 200 mg of polyethylene glycol (PEG, Mw 20 000) and 180 mg of copper(II) chloride dehydrate ( $\text{CuCl}_2 \cdot 2\text{H}_2\text{O}$ ) were dissolved in 200 mL  $\text{H}_2\text{O}$ , which was stirred with a magnetic stirrer. This solution was stirred for 30 min to ensure that the PEG and  $\text{CuCl}_2$  completely dissolved. Then, 2 mL of 6 M NaOH was added dropwise to the solution of  $\text{CuCl}_2$  and PEG under constant stirring. A blue precipitate of  $\text{Cu}(\text{OH})_2$  was rapidly produced. After stirring for 30 min, 2 mL of a 14 M solution of hydrazine ( $\text{N}_2\text{H}_4 \cdot \text{H}_2\text{O}$ ) was added dropwise to the solution with the blue  $\text{Cu}(\text{OH})_2$  precipitate under constant stirring for 30 min to reduce  $\text{Cu}^{2+}$  to  $\text{Cu}^{1+}$ . The  $\text{Cu}(\text{OH})_2$  precipitate gradually turned red. After the  $\text{Cu}(\text{OH})_2$  precipitate was completely reduced by the  $\text{N}_2\text{H}_4$ , the red gel was transferred into an autoclave and was heated for 10 h at different temperatures (80, 100, 120 and 140 °C). The produced precipitates were filtered, were washed with distilled water several times, and were dried in a vacuum oven at 60 °C for 3 h.

### 2.2. Characterization techniques

X-ray diffraction (XRD) analysis was performed at room temperature with a Bruker AXS D8 with  $\text{Cu K}\alpha$  radiation ( $\lambda = 1.540 \text{ \AA}$ ) over a  $2\theta$  collection range of 10–80°.

The specific surface area was calculated from measurements of  $\text{N}_2$  adsorption with a Nova 2000 series Chromatech apparatus at 77 K. Prior to the measurements all samples were treated under vacuum at 200 °C for 2 h.

The band gap of the samples was identified from UV–vis diffuse reflectance spectra (UV–vis-DRS) in air at room temperature from 200–800 nm with an UV/vis/NIR spectrophotometer (V-570, JASCO, Japan).

Transmission electron microscopy (TEM) was recorded with a JEOL-JEM-1230 microscope; the samples were prepared by suspending the material in ethanol, then ultrasonically dispersing the suspension for 30 min, placing a small amount of this solution onto a carbon-coated copper grid and drying the solution before loading the sample in the TEM.

### 2.3. Photocatalytic test

The application of the synthesized nanocomposite to the photodegradation of pure DB53 dye was investigated under visible light. The experiments were performed in a cylindrical Pyrex glass cell with an effective volume of 400 mL, and the irradiation source was placed outside the reactor. The photocatalyst was irradiated with a blue fluorescent lamp (150 W) covered by two UV cut filters. The intensity of the UV light was confirmed to be less than the detection limit (0.1 mW/cm<sup>2</sup>) of a UV radiometer. In a typical experiment, 0.4 gm of catalyst was suspended in 300 mL of 100 mg/L pure DB53 dye solution (pH ~ 7). The reaction was performed isothermally at 25 °C through use of a circulating supply of cooling water. Prior to irradiation, the solution was stirred and was bubbled with oxygen for at least 60 min in the dark to allow the system to reach equilibrium so that the loss of compound from adsorption can be considered. The suspension was continuously purged with bubbling oxygen throughout the experiment. Samples of the reaction mixture were acquired at different intervals and the catalyst was removed from the liquid phase by filtration through nylon syringe filters (pore size: 0.45  $\mu\text{m}$ ).

The concentration of the unreacted Direct Blue dye was analyzed with the UV JASCO (V 570) at  $\lambda_{\text{max}} = 612 \text{ nm}$ .

The percent of DB53 dye removed was measured by applying the following equation:

$$\% \text{ Removal efficiency} = (\text{Co} - \text{C}) / \text{Co} \times 100$$

where Co is the initial concentration of DB53 in solution and C is the remaining concentration in solution after reaction.

For comparison,  $\text{TiO}_2$  Degussa P25 was tested for the photocatalytic degradation of Direct Blue dye under the same conditions.

## 3. Results and discussion

### 3.1. X-Ray diffraction analysis

Fig. 1 shows the XRD patterns of  $\text{Cu}_2\text{O}$  samples prepared at different hydrothermal temperatures of 80, 100, 120 and 140 °C. The four patterns in Fig. 1 are found to be consistent with the cuprite structure of  $\text{Cu}_2\text{O}$  (JCPDS card No. 05-0667). As the hydrothermal temperature increased, the diffraction peaks of the products gradually became narrow and sharp. This change indicates that the crystallinity of the produced  $\text{Cu}_2\text{O}$  increased and that the crystallite size grew as hydrothermal temperature increased. The mean

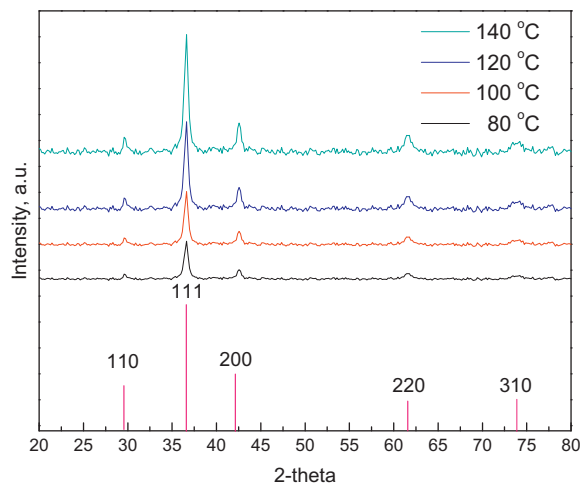


Fig. 1. XRD patterns of  $\text{Cu}_2\text{O}$  samples prepared at different hydrothermal temperatures.

Table 1

Crystallite size, BET surface area, band gap energy and rate constant for the reaction of Direct Blue dye with the  $\text{Cu}_2\text{O}$  samples prepared at different hydrothermal temperatures.

Hydrothermal temperature (°C)	Crystallite size (nm)	$S_{\text{BET}}$ ( $\text{m}^2/\text{g}$ )	Band gap energy (eV)	$k \times 10^{-4}$ ( $\text{min}^{-1}$ )
80	19.3	40.1	2.00	330
100	26.0	32.1	2.16	190
120	26.8	20.1	2.36	150
140	31.5	13.4	2.63	100

crystallite size can be roughly determined from the broadening of the peaks through the Scherrer formula. From fits of the full width at half maximum (FWHM) of the (111) peaks to this formula, the mean sizes of the  $\text{Cu}_2\text{O}$  samples at different hydrothermal temperatures (80, 100, 120 and 140 °C) were found to be 19.3, 26.0, 26.3 and 31.5 nm, respectively (Table 1).

### 3.2. TEM observation

TEM images of the  $\text{Cu}_2\text{O}$  samples prepared under different hydrothermal temperatures are displayed in Fig. 2.  $\text{Cu}_2\text{O}$ , prepared at a hydrothermal temperature of 80 °C, consists of nearly homogeneous nanorods (Fig. 2a). On increasing the hydrothermal temperature to 100, 120 and 140 °C, the phases of the produced  $\text{Cu}_2\text{O}$  are a mixture of nanorods and nanocubes, a mixture of nanorods and nanocubes and nanocubes, respectively (Fig. 2b, c and d). Therefore, the hydrothermal temperature plays an important role in determining the obtained phase of the produced  $\text{Cu}_2\text{O}$ .

### 3.3. Specific surface area analysis

The  $\text{N}_2$  adsorption–desorption measurement at a liquid  $\text{N}_2$  temperature of  $-196 \text{ }^\circ\text{C}$  was used to study the mesoporosity and textural properties of the synthesized  $\text{Cu}_2\text{O}$  samples. Fig. 3 depicts the  $\text{N}_2$  adsorption–desorption isotherm of the prepared samples. In Fig. 3, the isotherm shows typical type II sorption behavior; therefore, the hydrothermal temperature does not affect the type of isotherm. The surface areas of the products are listed in Table 1. The surface area of the  $\text{Cu}_2\text{O}$  obtained at a hydrothermal temperature of 80 °C is 40.1  $\text{m}^2/\text{g}$ . As the hydrothermal temperature increases, the surface area is greatly reduced from 41.1  $\text{m}^2/\text{g}$  at

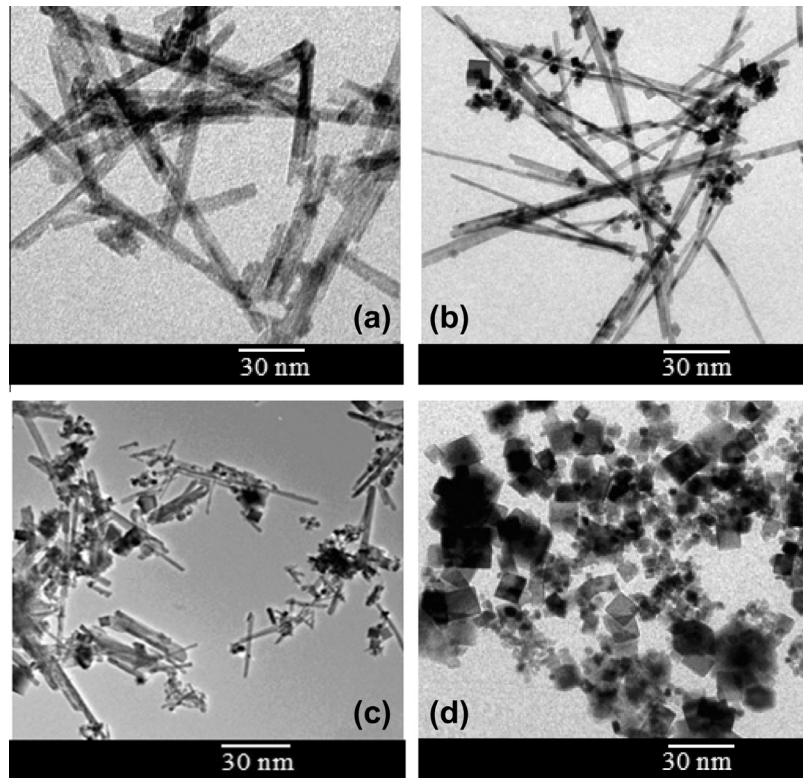


Fig. 2. TEM images of the  $\text{Cu}_2\text{O}$  samples prepared at different hydrothermal temperatures.

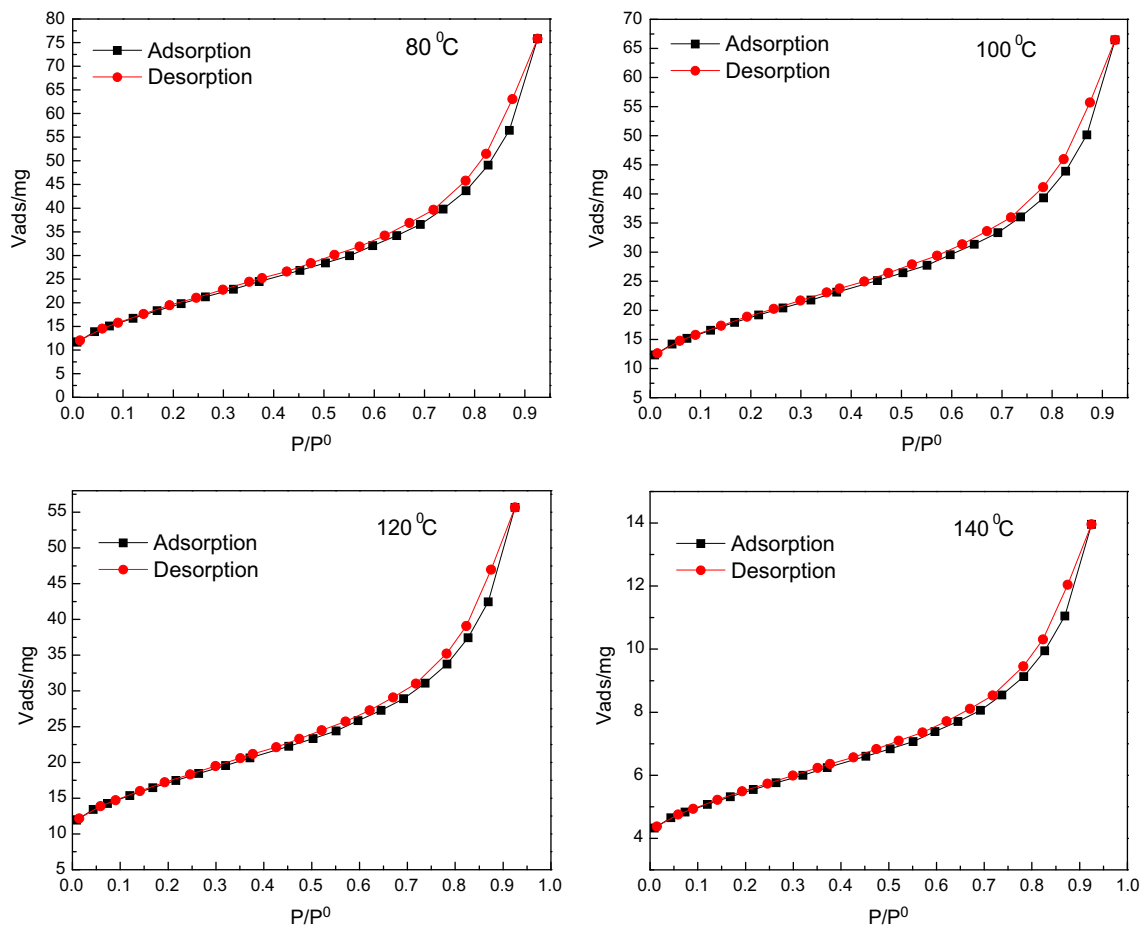


Fig. 3.  $\text{N}_2$  sorption isotherms of the  $\text{Cu}_2\text{O}$  samples prepared at different hydrothermal temperatures.

80 °C to 13.4 m<sup>2</sup>/g at 140 °C. Therefore, the hydrothermal temperature plays an important role in determining the specific surface area of the produced Cu<sub>2</sub>O.

#### 3.4. UV–vis absorption spectra

Fig. 4 shows the UV–vis spectra of the Cu<sub>2</sub>O prepared at different hydrothermal temperatures. The results reveal that the absorbance edges of the Cu<sub>2</sub>O products regularly varied. As the hydrothermal temperature increased, the absorbance edges of the products moved gradually to shorter wavelength. In other words, as the hydrothermal temperature decreases, a blue shift occurs; this blue shift primarily resulted from quantum size effects in the nanosystem. Obviously, with increasing hydrothermal temperature, the position of the absorption peak of the as-synthesized Cu<sub>2</sub>O samples shifted considerably to lower wavelengths. This behavior is typical of the quantum size effect in the nanosystem. An estimate of the optical band gap is obtained with the following equation:

$$\alpha(h\nu) = A(h\nu - E_g)^{m/2}$$

where  $A$  is a constant,  $\alpha$  is the absorption coefficient, and  $m$  equals 1 for a direct transition. The energy intercept of a plot of  $(\alpha h\nu)^2$  as a function of  $(h\nu)$  yields  $E_g$  for a direct transition [41]. The band gap values calculated for the prepared samples are presented in Table 1. The results show a gradual narrowing of the band gap of the prepared samples as the hydrothermal temperature decreases, and in turn, this narrowing increases the absorbency in the visible light region. Therefore, the hydrothermal temperature plays an important role in determining the band gap of the produced Cu<sub>2</sub>O.

#### 3.5. Photocatalytic activity analysis

Fig. 5 shows the photocatalytic degradation of a Direct Blue dye solution with the Cu<sub>2</sub>O catalysts from different hydrothermal temperatures and P<sub>25</sub> under visible light and dark conditions. The solutions degraded gradually with prolonged irradiation times. After 60 min, complete photocatalytic degradation of the Direct Blue dye solution was achieved by the sample prepared at a hydrothermal temperature of 80 °C (degradation = 100%). Comparatively, the photocatalytic degradation was approximately 88%, 80%, 69%, 17% and 3% for the samples prepared at 100, 120, 140 °C, for P<sub>25</sub> and under dark conditions, respectively. These results may arise from the reduction in the surface areas of the samples with increasing

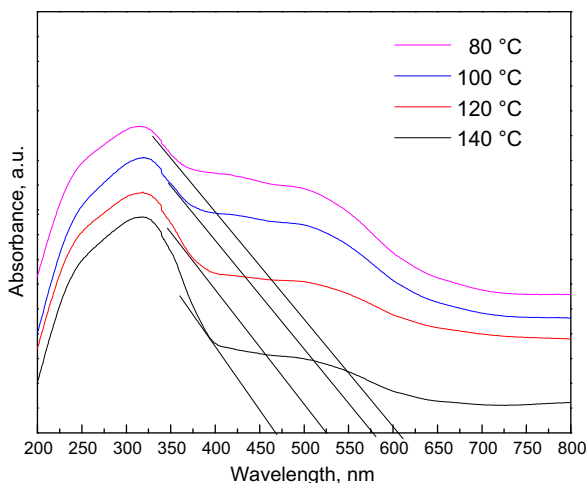


Fig. 4. UV–vis absorption spectra of the Cu<sub>2</sub>O samples prepared at different hydrothermal temperatures.

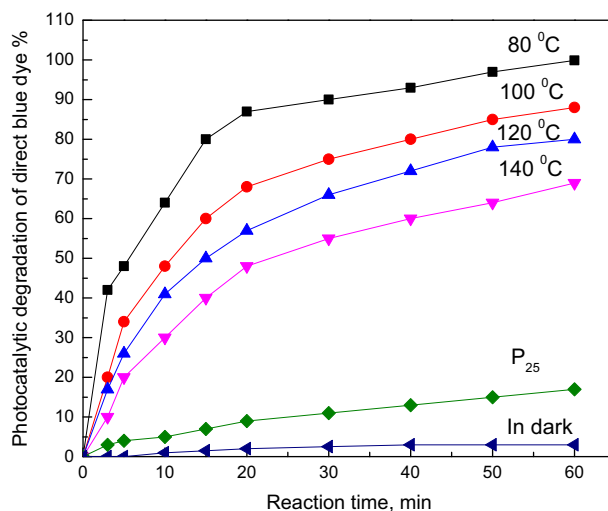


Fig. 5. Photocatalytic degradation of Direct Blue dye by Cu<sub>2</sub>O prepared at different hydrothermal temperatures, by P<sub>25</sub> and in the dark.

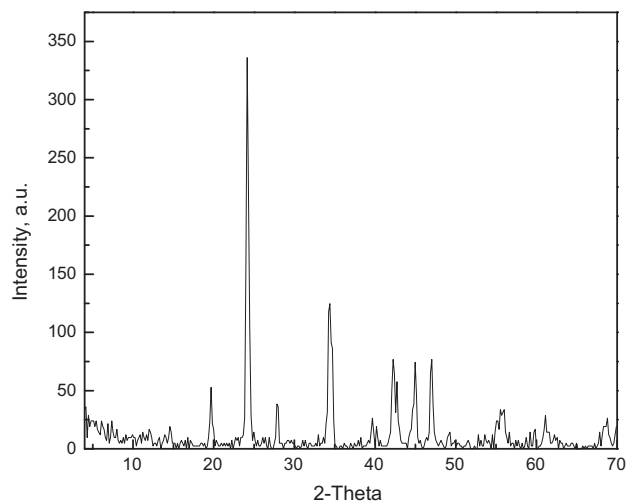


Fig. 6. XRD pattern of precipitate 1; the gas produced in the photocatalytic reaction was absorbed by an aqueous solution of NaOH (0.2 M) and Ba(NO<sub>3</sub>)<sub>2</sub> (0.2 M) was added to produce precipitate 1.

hydrothermal temperature, and this reduction leads to a decrease in the number of active sites on the surfaces of the particles. The low photocatalytic decomposition of Direct Blue dye by P<sub>25</sub> is because the reaction is performed under visible light and P<sub>25</sub> absorbs UV light; additionally, the adsorption of cyanide on the catalyst is very small, and the process that is occurring is photocatalysis.

To confirm the complete degradation of Direct Blue dye into carbon dioxide gas, the gases produced from the photocatalysis process were passed over a solution of 0.2 M NaOH for further analysis. Then, barium nitrate solution was added, and the resulting white precipitate was labeled precipitate 1. The XRD pattern of precipitate 1 is shown in Fig. 6. The pattern was assigned to BaCO<sub>3</sub> and is in good agreement with the standard card ICDD-PDF No. 05-0378. Therefore, the Direct Blue dye is completely oxidized to CO<sub>2</sub>.

The preceding UV–vis spectra showed that the absorbance edges of the Cu<sub>2</sub>O products are located in the range of 470–606 nm; therefore, the Cu<sub>2</sub>O can be excited by visible light and can generate electron–hole pairs. The mechanism for photocatalytic degradation of organic pollution on solid catalysts is always

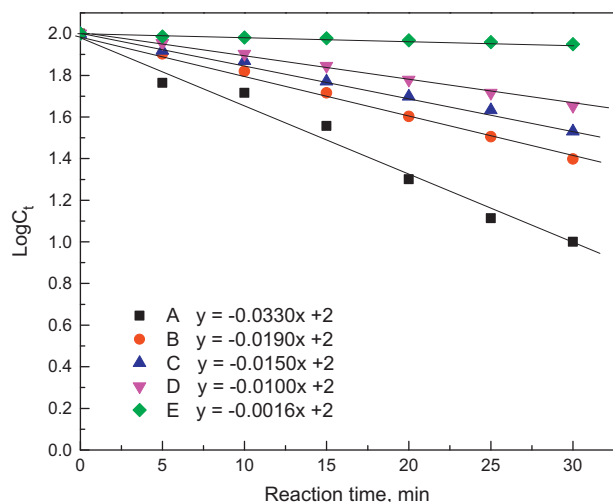
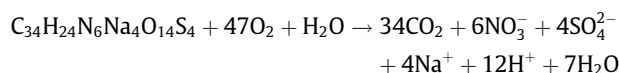
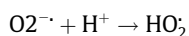
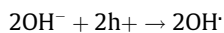
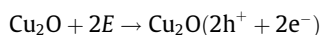


Fig. 7. Reaction kinetics for Direct Blue dye with  $\text{Cu}_2\text{O}$  prepared at 80 °C (A); 100 °C (B); 120 °C (C); 140 °C (D) and P25 (E).

depicted as follows: continuous band-gap irradiation of an aqueous semiconductor dispersion excites an electron from the valence band to the conduction band and creates an electron–hole pair. The photogenerated holes are considered to be capable of directly oxidizing many organic compounds. However, recombination of the electron–hole pairs will decrease the photocatalytic activity. Initially, in our experiments, when the grain size is as small as 19.3 nm, the photogenerated carriers diffuse quickly from center to the surface [42], resulting in higher separation efficiency for the photogenerated electron–hole pairs and higher photocatalytic activity for the particles. Second, the increase in the specific surface area leads to an increase in the ability to adsorb organics and maximizes the ability to photocatalytically degrade organics. Therefore, as the grain size of the  $\text{Cu}_2\text{O}$  decreases and consequently the specific surface area increases, the photocatalytic degradation property of  $\text{Cu}_2\text{O}$  is improved. The photocatalyst was utilized to repeatedly photodegrade Direct Blue dye under visible light. The photocatalytic performance was 100% over the first 6 cycles. The photocatalytic activity of the recycled photocatalyst decreased by 4% after 7 cycles. The results show that the separation of the photocatalyst was effective, and the persistence of the photocatalytic activity of the  $\text{Cu}_2\text{O}$  was promising.

$\text{Cu}_2\text{O}$  is a semiconductor which can be excited to a higher energy state by receiving light energy; electrons are released from the illuminated surface of  $\text{Cu}_2\text{O}$  and jump to the conduction band, leaving a hole in valence band. The hole in the valence band is strongly oxidizing and removes an electron from  $\text{OH}^-$  (hydroxide ion) in water; simultaneously,  $\text{OH}^-$  takes an electron and becomes a very unstable  $\text{OH}^\cdot$  radical. Through strong oxidation, the  $\text{OH}^\cdot$  radical takes an electron from a nearby organic compound to become stable. In this way, the organic compound is decomposed by electron loss, is finally converted to  $\text{CO}_2$  and water and is released into the atmosphere. The following equations illustrate the possible photocatalytic reaction mechanisms that may take place in our catalytic system.



where  $E$  is the energy.

### 3.6. Kinetics of Direct Blue dye with $\text{Cu}_2\text{O}$

At different hydrothermal temperatures, the reaction order with respect to Direct Blue dye was determined by plotting the reaction time as a function of the log [Direct Blue dye], based on the following equation:

$$\text{Log}[C]_t = -kt + \text{Log}[C]_0$$

where  $[C]_0$  and  $[C]_t$  represent the concentration of substrate in solution before illumination and after illumination for time  $t$ , respectively, and  $k$  represents the apparent rate constant ( $\text{min}^{-1}$ ). The findings are presented in Fig. 7, and the apparent rate constants are summarized in Table 1. The results show that the reaction followed first-order kinetics with respect to Direct Blue dye and the rate constants were in the range of  $100 \times 10^{-4}$  to  $330 \times 10^{-4} \text{ min}^{-1}$  for the different hydrothermal temperatures and  $16 \times 10^{-4} \text{ min}^{-1}$  for P25 Degussa. Therefore, the rate constant for  $\text{Cu}_2\text{O}$  prepared at a hydrothermal temperature of 80 °C is 20 times larger than that for P25 under visible light. The first-order rate equation for Direct Blue dye is given by  $R = k [\text{Direct Blue dye}]$ .

## 4. Conclusions

A simple hydrothermal route was used to synthesize shape-controllable  $\text{Cu}_2\text{O}$  from starting materials of  $\text{CuCl}_2 \cdot 2\text{H}_2\text{O}$  and  $\text{NaOH}$  by changing the hydrothermal temperature from 80 to 140 °C.  $\text{Cu}_2\text{O}$  exists as a nanorod and has a surface area of  $40.1 \text{ m}^2/\text{gm}$  and a band gap of 2.00 eV if the hydrothermal temperature is 80 °C. Therefore, the hydrothermal temperature plays an important role in determining the shape, surface area and band gap of the produced  $\text{Cu}_2\text{O}$ . Measurements of the photocatalytic degradation of a Direct Blue dye solution showed that  $\text{Cu}_2\text{O}$  nanorods exhibited highly active and efficient photocatalytic properties for water purification and may find potential applications in related fields. The catalyst could be reused with no loss of activity over the first 6 cycles. The degradation efficiency for Direct Blue dye was still high, approximately 96%, after the photocatalyst was used six times.

## Acknowledgements

This paper was funded by the Deanship of Scientific Research (DSR), King Abdulaziz University, Jeddah, under grant number (11-130-D1432). The authors, therefore, acknowledge with thanks the technical and financial support from the DSR.

## References

- [1] R.M. Mohamed, E.S. Baeissa, J. Alloys Comp. 558 (2013) 68–72.
- [2] R.M. Mohamed, M.M. Mohamed, Appl. Catal. A 340 (2008) 16–24.
- [3] R.M. Mohamed, Desalination Water Treat. 50 (2012) 147–156.
- [4] H. Yan, S.T. Kochuveedu, Li Na Quan, Sang S. Lee, D.Ha Kim, J. Alloys Comp. 560 (2013) 20–26.
- [5] Y. Cao, Z. Zhao, J. Yi, C. Ma, D. Zhou, R. Wang, C. Li, J. Qiu, J. Alloys Comp. 554 (2013) 12–20.
- [6] R.M. Mohamed, E.S. Aazam, Chin. J. Catal. 33 (2012) 247–253.
- [7] R.M. Mohamed, E.S. Aazam, J. Alloys Comp. 509 (2011) 10132–11038.
- [8] H. Zhang, C. Liang, J. Liu, Z. Tian, G. Wang, W. Cai, Langmuir 28 (2012) 3938–3944.
- [9] R. Liu, P. Wang, X. Wang, H. Yu, J. Yu, J. Phys. Chem. C 116 (2012) 17721–17728.
- [10] R.M. Mohamed, E.S. Aazam, Int. J. Photoenergy (2011) 7 (Article ID 137328).

- [11] R.M. Mohamed, I.A. Mkhaldid, *J. Alloys Comp.* 501 (2010) 301–306.
- [12] K. Chen, X. Feng, R. Hu, Y. Li, K. Xie, Y. Li, H. Gu, *J. Alloys Comp.* 554 (2013) 72–79.
- [13] R.M. Mohamed, I.A. Mkhaldid, *J. Alloys Comp.* 501 (2010) 143–147.
- [14] R.M. Mohamed, L.D. Mickinny, M.W. Sigmund, *Mater. Sci. Eng. R* 73 (2012) 1–13.
- [15] R.M. Mohamed, K. Mori, H. Yamashita, *Int. J. Nanoparticles* 2 (2009) 533–542.
- [16] K.H. Yoon, W.J. Choi, D.H. Kang, *Thin Solid Films* 372 (2000) 250–256.
- [17] M. Hara, T. Kondo, M. Komoda, S. Ikeda, K. Shinohara, A. Tanaka, J.N. Kondo, *Chem. Commun.* (1998) 357–358.
- [18] S. Ikeda, T. Takata, T. Kondo, G. Hitoki, Michikazu Hara, Junko N. Kondo, Kazunari Domen, Hideo Hosono, Hiroshi Kawazoe, Akira Tanaka, *Chem. Commun.* (1998) 2185–2186.
- [19] C.A.N. Fernando, T.M.W.J. Bandara, S.K. Wethasingha, *Sol. Energy Mater. Sol. Cells* 70 (2001) 121–129.
- [20] C.C. Hu, J.N. Nian, H. Teng, *Sol. Energy Mater. Sol. Cells* 920 (2008) 1071–1076.
- [21] S. Jing, S. Xing, Y. Wu, Y. Wang, B. Zhao, C. Zhao, *Mater. Lett.* 61 (2007) 2281–2283.
- [22] Y.S. Luo, Y. Tu, Q. Ren, X. Dai, L. Xing, J. Li, *J. Solid State Chem.* 182 (2009) 182–186.
- [23] A. Tang, Y. Xiao, J. Ouyang, S. Nie, *J. Alloys Comp.* 457 (2008) 447–451.
- [24] H. Yang, J. Ouyang, A. Tang, Y. Xiao, X. Li, X. Dong, Y. Yu, *Mater. Res. Bull.* 41 (2006) 1310–1318.
- [25] W. Liang, M. Bockrath, D. Bozovic, J.H. Hafner, M. Tinkham, H. Park, *Nature* 411 (2001) 665–669.
- [26] J. Yu, J.C. Yu, W. Ho, L. Wu, X. Wang, *J. Am. Chem. Soc.* 126 (2004) 3422–3423.
- [27] S.S. Chang, C.W. Shih, C.D. Chen, W.C. Lai, C.R.C. Wang, *Langmuir* 15 (1999) 701–709.
- [28] Y. Lei, L.D. Zhang, J.C. Fan, *Chem. Phys. Lett.* 338 (2001) 231–236.
- [29] J.J. Shiang, A.V. Kadavanich, R.K. Grubbs, A.P. Alivisatos, *J. Phys. Chem.* 99 (1995) 17417–17422.
- [30] C. Kittel, *Introduction to Solid State Physics*, Wiley, New York, 1986.
- [31] D.A. Tryk, A. Fujishima, K. Honda, *Electrochim. Acta* 45 (2000) 2363–2376.
- [32] T. Takata, S. Ikeda, A. Tanaka, S. Hara, J.N. Kondo, K. Domen, *Appl. Catal. A: Gen.* 200 (2000) 255–262.
- [33] B.P. Rai, *Phys. Status Solidi A* 99 (1987) k35–k39.
- [34] P. Poizot, S. Laruelle, S. Grugeon, L. Dupont, J.-M. Tarascon, *Nature* 407 (2000) 496–499.
- [35] J. Ramírez-Ortiz, T. Ogura, J. Medina-Valtierra, S.E. AcostaOrtiz, P. Bosch, J.A. de los Reyes, V.H. Lara, *Appl. Surf. Sci.* 174 (2001) 177–184.
- [36] W.Z. Wang, G.H. Wang, X.S. Wang, *Adv. Mater.* 14 (2002) 67–69.
- [37] L. Huang, H. Wang, Z. Wang, *Chem. Mater.* 14 (2002) 876–880.
- [38] J. Oh, Y. Tak, Y. Lee, *Electrochem. Solid State* 7 (2004) C27–C30.
- [39] W.Z. Wang, O.K. Varghese, C.M. Ruan, M. Paulose, C.A. Grimes, *J. Mater. Res.* 18 (2003) 2756–2759.
- [40] M. Cao, C. Hu, Y. Wang, Y. Guo, C. Guo, E. Wang, *Chem. Commun.* (2003) 1884–1885.
- [41] J. Miaoa, H. Wanga, Y. Lia, J. Zhu, J.-jie Zhu, *J. Cryst. Growth* 281 (2005) 525–529.
- [42] H. Xu, H. Wang, H. Yan, *J. Hazard. Mater.* 144 (2007) 82–85.